Deflective signal analysis in photothermal measurements in the frame of complex geometrical optics

Roman J. BUKOWSKI, Dorota KORTE

Institute of Physics, Silesian University of Technology, ul. Bolesława Krzywoustego 2,
44-100 Gliwice, Poland

The influence of one dimensional plane thermal wave on probing Gaussian beam phase and deflection by complex geometrical optics methods has been analyzed in the work. The probing beam detection by quadrant photodiode has been investigated. The dependence of photodiode current signal on the probing beam diameter, its waist, sample position, angular modulation frequency and the height of the beam over the sample has been studied.

Keywords: complex geometrical optics, mirage effect, preturbation calculus, deflectional detection, thermal waves, Gaussian beams, geometrical optics of nonhomogeneus media, phase change and deflection.

1. Introduction

Nowadays, investigations of solid state thermal properties have great importance, especially for different nonhomogeneous layered systems. Among them the most essential are those photothermal methods that are based on differences between thermal properties of different parts of that layered system. Temperature changes in such a system are measured directly or indirectly and on this principle we can conclude about its structure.

One of the indirect methods for measuring sample surface temperature changes is photodeflective method. In this method, the periodically heated sample changes the temperature of surrounding gas, and next it changes the gas refraction index. The last changes are detected by probing light beam with known light intensity distribution passing through the heated gas layer. Changes in the gas refraction index cause deflection and phase change in the probing beam.

At present two theoretical methods for description of these phenomena are used [1, 2]. The first one is the ray method. It is based on the small shift of light beam (deflection) in optically nonhomogeneous media. There is also a generalization of that method to wide probing beams [3, 4]. The second method is the wave one [2]. In this work, the wave equation was solved for the probing beam propagation but only its phase change was taken under consideration.

A complete (with arbitrary accuracy) description of light beam propagation in optically nonhomogeneous medium can be found in the frame of geometrical optics method by the use of Debye's expansion [5–7]. The proper analysis using complex geometrical optics methods and taking into account only the phase change of probing light beam, caused by thermal waves, was presented in [7, 8].

All of the works quoted assumed that deflection of probing beam is registered by the use of quadrant photodiode, from which we can obtain two signals: normal and tangential one. The first one responds to illumination difference between upper and lower and the second one between left and right photodiode halves (defined relatively to the "horizontal" surface of the sample under investigation). In real experimental situation the thermal field in the gas over the sample because the pumping beam or sample heterogeneity is 3-dimensional. This type of thermal field was presented in some works, *e.g.*, [3]. In this situation, both normal and tangential parts are present in the deflective measurements. In this work, we present a new method for calculating the influence of thermal field on the probing Gaussian beam parameter. For good presentation of this method we use a rather simple shape of thermal field. If the sample stimulation is much wider than the width of the probing beam, the theoretical description is one-dimensional and only the normal signal is important.

2. Gaussian beam in an optically homogeneous medium

From work [6] it follows, that the electric field distribution in Gaussian beam with radius a and wavelength λ (wave number $k = 2\pi/\lambda$) which propagates in homogeneous medium with refraction index n_0 can be written as:

$$u(x, y, z) = A_0(\mathbf{r}) \exp\left(ik\psi_0(\mathbf{r}) \right) \tag{1}$$

where

$$A_0(\mathbf{r}) = E_0\left(1 + \frac{i(z - L)}{z_R} \right)^{-1},$$

$$\tag{2}$$

$$\psi_0(\mathbf{r}) = (z - L)n_0 + in_0\frac{x^2 + y^2}{2z_R}\left(1 + \frac{i(z - L)}{z_R} \right)^{-1}.$$

The beam enters the system on the plane $z = 0$ and propagates in the plus direction of the OZ axis, and its waist is placed on the plane $z = L$. E_0 is the electric field intensity in the middle of the waist. The parameter $z_R = ka^2n_0$ is called Rayleigh's length, the quantity ψ_0 – wave eikonal and A_0 – its amplitude (of zero order). The beam ray coordinates $\mathbf{r}(\tau) = [x(\tau), y(\tau), z(\tau)]$ are defined by equations:

$$x(\tau) \;=\; \xi + i\xi\frac{n_0\tau}{z_{RC}},$$

$$y(\tau) \;=\; \eta + i\eta\frac{n_0\tau}{z_{RC}}, \tag{3}$$

$$z(\tau) \;=\; n_0\tau\sqrt{1 + \frac{\xi^2 + \eta^2}{z_{RC}^2}}$$

where $[\xi, \eta]$ are the ray start point coordinates from the plane $z = 0$ (*XY*), $z_{RC} = z_R - iL$ and τ is the running coordinate (in general case the complex one) along the ray. It is easy to notice that relations (3) represents straight lines in 6-dimensional complex space.

For a given observation point $\mathbf{r_D} = [x_D, y_D, z_D]$ (*e.g.*, point on the detection plane) we need to find all rays coming to that point. For this purpose, a solution of the set of Eq. (3), relatively to "rays" variable $[\xi, \eta, \tau]$, needs to be found (the so-called geometrical optics reversal problem). After linearization we get:

$$\xi_D \cong x_D\left(1 + \frac{iz_D}{z_{RC}}\right)^{-1},$$

$$\eta_D \cong y_D\left(1 + \frac{iz_D}{z_{RC}}\right)^{-1}, \tag{4}$$

$$\tau_D \cong \frac{z_D}{n_0}\left(1 - \frac{\xi^2 + \eta^2}{2z_{RC}^2}\right) \cong \frac{z_D}{n_0}.$$

From this solution it follows, that for this simplification we have a particularly simple situation – to all observation points there comes only one ray. Equations (4) define exactly the start point of the ray (ξ_D, η_D) when its observation point (x_D, y_D, z_D) is known.

3. Gaussian beam in a thermally disturbed medium

Let us consider a standard experimental set-up scheme for the solid state photothermal investigation with photodeflective detection (Fig. 1). Modulated light beam is incident on the sample and gives it periodically specified energy flux. As a result, the sample
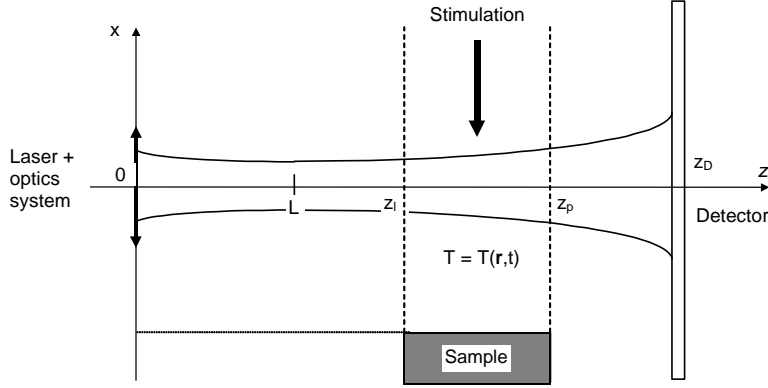
Fig. 1. Experimental set-up scheme for solid state investigation by photothermal method with photodeflectional detection. The gas heated region have the width $\Delta z = z_p - z_l$ and its left edge distance from the set-up beginning (light beam "input") is equal z_l. We assume that the heated region width along the OY axis is much more greater then the probing light beam diameter. The light beam radius in their waist is equal a and it is placed at distance L from the "input". The screen (detector) is placed at distance z_D from the light beam "input".

and surrounding gas (*e.g.*, air) are heated and in stationary state we deal with periodical temperature changes in time and space, so-called thermal waves. In typical photo-thermal measurements, the total increase of sample temperature is of the order of fraction of Kelvin and changes in temperature amplitude are about an order smaller. The temperature field of the thermal wave in gas above the sample can be written as:

$$\vartheta_g(x, t) = a_g + b_g \exp(-k_g x) \cos(\Omega t - k_g x + \varphi_g) \tag{5}$$

where a_g – constant rise of gas temperature, b_g – amplitude of the sample surface temperature, φ_g – phase shift between the sample surface temperature and stimulation beam, $k_g = (\Omega/2\kappa_g)^{1/2}$ – wave number of the thermal wave (equal to its attenuation coefficient), κ_g – thermal diffusivity of gas, Ω – angular frequency of modulation. The quantities a_g, b_g and φ_g depend on some thermal and geometrical parameters of the gas and the sample and are not considered here.

These thermal waves cause changes in the gas refraction index [9–11], which gives rise to modification of the probing beam parameters. In the first approximation we can assume that

$$n(T) \cong n_0 + \left.\frac{dn}{dT}\right|_{T_0} (T - T_0) = n_0 + n_0 s_T (T - T_0), \quad T_0 = \text{const}(\mathbf{r}) \tag{6}$$

where n_0 – gas refraction index at temperature T_0, $s_T = \left.\dfrac{1}{n_0} \dfrac{dn}{dT}\right|_{T_0}$ – refraction index

thermal sensitivity. In such a situation, the dielectric constant of the medium in the thermally changed region is expressed by the equation

$$\varepsilon(T) = n^2(T) \cong n_0^2 + 2n_0^2 s_T \Big(T(\mathbf{r}) - T_0 \Big) = n_0^2 + \nu(\mathbf{r}). \tag{7}$$

Changes in the probing beam are expressed by ν.

4. Gaussian beam deflection in the thermal wave field

The Gaussian beam deflection is one of the effects of its propagation in the thermally disturbed medium. This means that the ray trajectory change in the thermal wave field must be found. Because of the fact that temperature distribution is merely a function of variable x, only this coordinate of the ray trajectory is changed. The other ray coordinates are described by the second and the third equations in (4). The first correction to the ray x coordinate is given by [5]:

$$\mathbf{r_1} = \mathbf{r_1^0} + \mathbf{p_1^0}\tau + \int_0^\tau (\tau - \tau')\frac{1}{2}\nabla \nu\Big(\mathbf{r}_0(\tau')\Big)d\tau' \tag{8}$$

which gives (after regarding (7) and boundary conditions) correction to x ray-coordinate (see Appendix 1):

$$x_1(\xi, \tau) = n_0^2 s_T \int_0^\tau (\tau - \tau')\frac{\partial \vartheta_g}{\partial x}d\tau' \cong (\tau - \tau_s)P(\xi)\tau_{pl}, \tag{8a}$$

$$P(\xi) = \sqrt{2}\, n_0^2 s_T\, b_g\, k_g \exp\Big(-k_g x_0(\tau_s)\Big) \sin\Big(\Omega t - k_g x_0(\tau_s) + \varphi_g - \frac{\pi}{4}\Big), \tag{8b}$$

$$\tau_s = \frac{1}{2}\Big[(\tau + \tau_l)H(\tau - \tau_l) - (\tau - \tau_p)H(\tau - \tau_p)\Big],$$

$$\tau_{pl} = (\tau - \tau_l)H(\tau - \tau_l) - (\tau - \tau_p)H(\tau - \tau_p),$$

$$\tau_l = \frac{z_l}{n_0}, \qquad \tau_p = \frac{z_p}{n_0}.$$

<div align="right">(8c)</div>

Above, we use $H(\tau)$ – Haeviside's step function. Finally, the perturbed ray coordinates are then

$$x(\xi, \tau) = x_0(\xi, \tau) + x_1(\xi, \tau) = \xi_0 \left(1 + i \frac{n_0 \tau}{z_{RC}} \right) + P(\xi)(\tau - \tau_s) \tau_{pl},$$

$$y(\xi, \tau) = y_0(\xi, \tau), \tag{9}$$

$$z(\xi, \eta, \tau) = z_0(\xi, \eta, \tau).$$

5. Gaussian beam phase change in the thermal wave field

The Gaussian beam eikonal can be written as [5]:

$$\psi(\tau) = \psi^0(\tau) + \int\limits_0^\tau \varepsilon(\mathbf{r}(\tau')) \mathrm{d}\tau'$$

$$\cong \psi^0(\tau) + \int\limits_0^\tau \varepsilon_0(\mathbf{r}(\tau')) \mathrm{d}\tau' + \frac{1}{2} \int\limits_0^\tau \nu(\mathbf{r}(\tau')) \mathrm{d}\tau'$$

$$= \psi_0 + \psi_1 \tag{10}$$

where integration is carried along the corrected probing beam ray (9).

Finally, correction to the eikonal is given in the form:

$$\psi_1 = z n_0 \frac{x_D}{z_{RC}^2} (\tau_D - \tau_s) P(\xi_0) \left(1 + i \frac{z_D}{z_{RC}} \right)^{-2} \tau_{pl} + a_g n_0^2 s_T \tau_{pl}$$

$$+ n_0^2 s_T b_g \tau_{pl} \exp(-k_g x(\xi, \tau_s)) \cos(\Omega t - k_g x(\xi, \tau_s) + \varphi_g) = \psi_{1d} + \psi_{1f} \tag{11}$$

where ψ_{1d} – the component (proportional to $P(\xi_0)$) that arises from Gaussian beam deflection in the thermal wave field, ψ_{1f} – the component resulting from the thermal field influence on the Gaussian beam phase (two terms proportional to a_g and b_g, respectively).

6. Gaussian beam ray amplitude change in the thermal wave field

The Jacobian of the transition from Cartesian to ray coordinates in the region $\tau > \tau_p$ is as follows (in paraxial approximation):

$$D(\tau) \cong \frac{\partial x}{\partial \xi} \frac{\partial y}{\partial \eta} \frac{\partial z}{\partial \tau}. \tag{12}$$

Using (9) we are given the probing beam amplitude changes expressed by the relation:

$$A(\tau) = A(0)\left[\frac{D(0)}{D(\tau)}\right]^{1/2} \cong E_0 \frac{z_R}{z_{RC}}\left(1 + i\frac{n_0\tau}{z_{RC}}\right)^{-1}\left[1 - \frac{1}{2}\frac{(\tau - \tau_s)\frac{\partial P}{\partial \xi}\tau_{pl}}{1 + i\frac{n_0\tau}{z_{RC}}}\right].$$

(13)

7. Normal signal from quadrant photodiode

The current normal signal from the photodiode under reverse bias is proportional to the light intensity incident on it (see Appendix 2). In such a case, the signal analyzed arises from the illumination difference between the upper and lower photodiode halves:

$$S_n = K_d \int\limits_{-\infty}^{\infty} dy_D \left(\int\limits_{0}^{\infty} - \int\limits_{-h}^{0}\right) dx_D I(\mathbf{r_D})$$

(14)

where K_d – photodetector constant (its sensitivity). In expression (14), it has been assumed that the sample curtains a part of the photodiode (in the region $-\infty < x_D < -h$).

In our case, when a lock-in nanovoltmeter is used for the diode current measurements, only $I_V(\mathbf{r_D})$ is measured. We have three different contributions to this signal, and due to this

$$S_n = S_{ndA} + S_{ndf} + S_{nf} = S_{nd} + S_{nf}.$$

(15)

After calculating proper integrals (see Appendix 2) we obtain

$$S_{nf} = A_f \cos(\Omega t + \varphi_g - \varphi_f),$$

$$S_{ndA} = A_{dA} \cos(\Omega t + \varphi_g + \varphi_{dA}),$$

(16)

$$S_{ndf} = A_{df} \cos\left(\Omega t + \varphi_g + \varphi_{df} - \frac{\pi}{4}\right).$$

The total deflective part of the signal is the sum of two last expressions in (16):

$$S_{nd} = S_{ndA} + S_{ndf} = A_d \cos(\Omega t + \varphi_g + \varphi_d),$$

(17)

$$A_d = \sqrt{\left[A_{dA}\cos\varphi_{dA} + A_{df}\cos\left(\varphi_{df} - \frac{\pi}{4} \right) \right]^2 + \left[A_{dA}\sin\varphi_{dA} + A_{df}\sin\left(\varphi_{df} - \frac{\pi}{4} \right) \right]^2}$$

(18)

$$\tan\varphi_d = \frac{A_{dA}\sin\varphi_{dA} + A_{df}\sin\left(\varphi_{df} - \frac{\pi}{4} \right)}{A_{dA}\cos\varphi_{dA} + A_{df}\cos\left(\varphi_{df} - \frac{\pi}{4} \right)}.$$

(19)

Finally, the full signal is the sum of the deflective and phasial components and it can be written in the form

$$S_{nt} = S_{nf} + S_{nd} = A_t\cos(\Omega t + \varphi_g + \varphi_t)$$

(20)

where

$$A_t = \sqrt{\left[A_d\cos(\varphi_g + \varphi_d) + A_f\cos(\varphi_g - \varphi_f) \right]^2 + \left[A_d\sin(\varphi_g + \varphi_d) + A_f\sin(\varphi_g - \varphi_f) \right]^2}$$

(21)

$$\tan\varphi_t = \frac{A_d\sin(\varphi_g + \varphi_d) + A_f\sin(\varphi_g - \varphi_f)}{A_d\cos(\varphi_g + \varphi_d) + A_f\cos(\varphi_g - \varphi_f)}.$$

(22)

8. Numerical calculations and graphs

Calculations were done for the interaction of He-Ne laser beam with thermal waves in air. The values of the parameters taken into account were as follows: sample width $z_p - z_l = 5$ mm, sample left edge position $z_l = 0.5$ m, sample right edge position $z_p = 0.505$ m, beam waist position $L = 0.5$ m, detector position $z_D = 1.5$ m, total power of probing beam $P_l = 1.0$ W ("normalized" value), wavelength of probing beam $\lambda = 636$ nm, gas refraction index at temperature T_0 was $n_0 = 1.0$, refraction index thermal sensitivity $s_T = 1.0$ K^{-1} ("normalized" value), our sample was silicon with thermal diffusivity $\kappa_s = 6.7{\times}10^{-5}$ m^2/s and thermal conductance $\lambda_s = 110$ W/(mK). The results of numerical calculations (formulas (21), (22) and (A2.17), (A2.18), (A2.23)) are presented in graphs with photothermal signal amplitude A_k [arb. u.] and additional phase shift φ_k [rad] (*i.e.*, relative to the temperature phase on the sample surface) dependence on some experimental set-up parameters. Here, $k = \{d, f, t\}$ relative to deflective or phasial component and total signal.

In the signal analyzed, as was mentioned in theoretical part of this work, two different parts were marked out – phasial and deflective ones. From experimental point
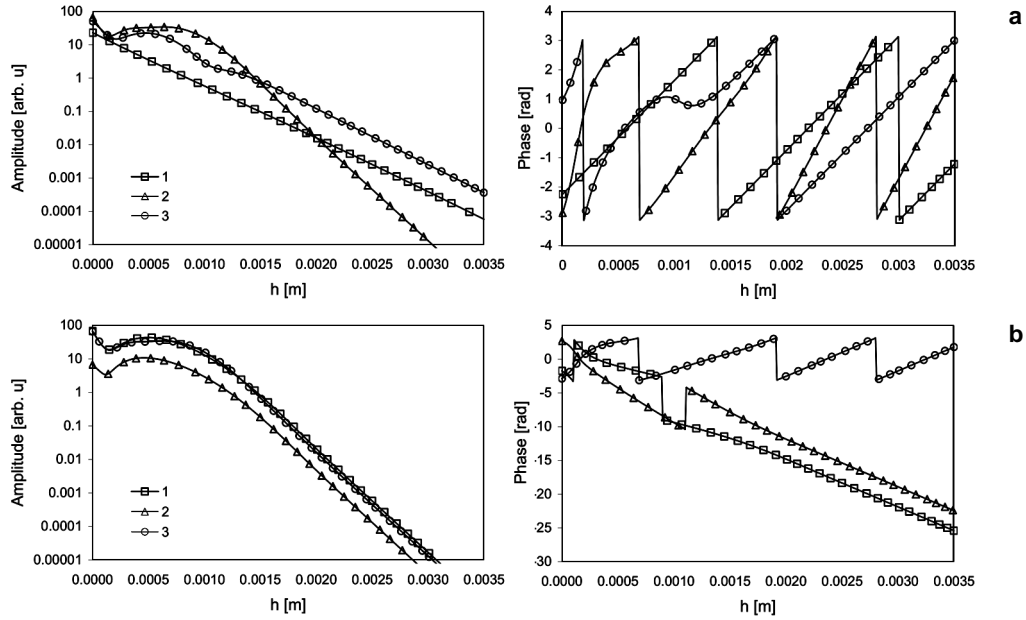
Fig. 2. Quadrant photodiode signal amplitude and additional phase shift changes relatively to probing beam height over the sample for: $\Omega = 600$ rad/s, $a = 50$ μm (curve 1); $\Omega = 2000$ rad/s, $a = 500$ μm (curve 2); $\Omega = 600$ rad/s, $a = 500$ μm (curve 3); others parameters are $z_D = 1.5$ m, $z_p = 0.505$ m, $z_l = 0.5$ m and $L = 0.5$ m – **a**. Components of the total normal signal: deflectional (curve 1) and phasial (curve 2) for $\Omega = 2000$ rad/s ($a = 500$ μm, $z_D = 1.5$ m, $z_p = 0.505$ m, $z_l = 0.5$ m and $L = 0.5$ m); curve 3 presents the total signal – **b**.

of view this differentiation is not essential and difficult to determine. But from theoretical point of view it is important, because as mentioned in the Introduction, two types of theoretical descriptions for deflective experimental analysis are used in literature. In all our calculations we determine both parts as well as the total signal and compare them. This enables us to determine the validity of the theory presented and those used in literature.

In typical photothermal measurements, the amplitude $A_k(h)$ and phase $\varphi_k(h)$ of photothermal signal dependence on distance between probing beam axis and illuminated sample (Fig. 2) are investigated. With an increase of the height of probing beam over the sample the signal dramatically decreases, which results from the fact that attenuation of the thermal wave is very strong in the medium. Analysing the graphs it can be concluded that the course of these curves is strongly dependent on both the probing beam diameter a and angular modulation frequency Ω. Figure 2**b** presents the shape of deflective and phasial components of photothermal signal.

Figure 3 presents the amplitude and phase of photothermal signal dependence on probing beam diameter for different angular modulation frequencies and heights of the probing beam over the sample. There is a value of the beam diameter for which the signal amplitude reaches a maximum. For small values of probing beam height
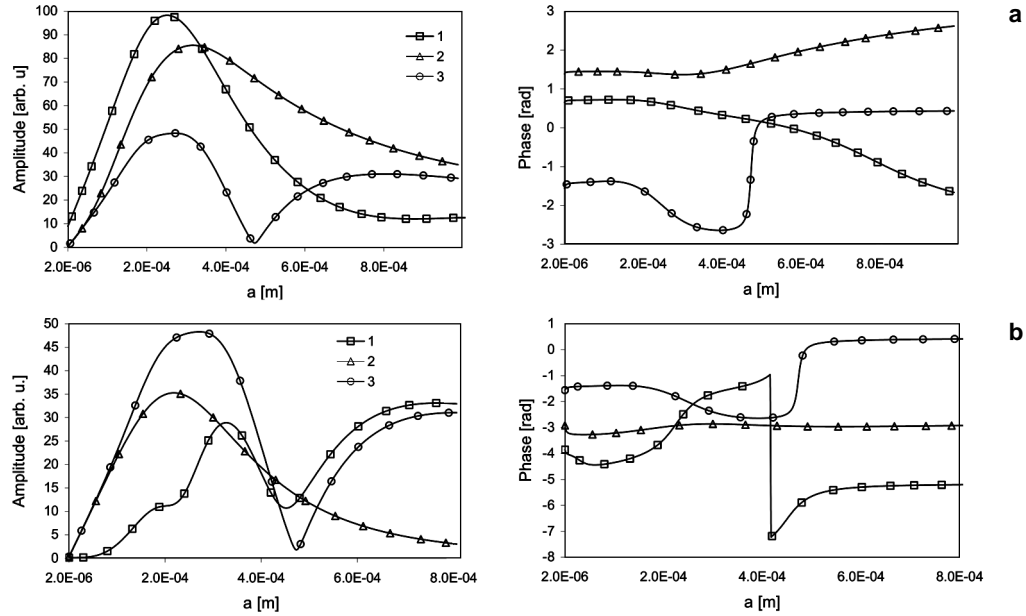
Fig. 3. Quadrant photodiode signal amplitude and additional phase shift changes relatively to probing beam diameter: $\Omega = 60$ rad/s, $h = 200$ µm (curve 1); $\Omega = 60$ rad/s, $h = 800$ µm (curve 2); $\Omega = 600$ rad/s, $h = 200$ µm (curve 3); others parameters are $z_D = 1.5$ m, $z_p = 0.505$ m, $z_l = 0.5$ m and $L = 0.5$ m – **a**. Components of the total normal signal: deflectional (curve 1) and phasial (curve 2) for $\Omega = 600$ rad/s, $h = 200$ µm (others parameters are $z_D = 1.5$ m, $z_p = 0.505$ m, $z_l = 0.5$ m and $L = 0.5$ m); curve 3 presents the total signal – **b**.

over the sample a minimum is also seen. The beams of small radius are wholly disturbed by thermal wave, while the beams of large *a* pass through the thermal field in different phase, which causes their phase shift. Because of that current signals from quadrant photodiode are also in different phase and they can extinguish each other. On the amplitude of photothermal signal dependance on probing beam diameter it can be seen as a minimum of the signal. For much larger values of *a* we enter the region in which the thermal wave is being declined, which means that the probing beam is not disturbed and the value of the signal decreases.

As can be seen from Fig. 4, the signal from quadrant photodiode rapidly decreases with an increase of angular modulation frequency for some values of *h* and *a* (curves 1 and 2). This arises from the fact that with an increase of frequency the thermal wave attenuation also increases. With an increase of frequency the temperature field gradient also increases, which causes an increase of deflective component of the total photothermal signal. This effect can be seen in curves 3 and 4. It is worth mentioning that the range of angular modulation frequency changes is determined by those values of Ω that are possible to attain using a mechanical modulator. With an increase of angular modulation frequency the thermal waves attenuation increases, and that is why very high values of Ω are not used in photothermal measurements.

Figure 5 presents the dependence of photothermal signal on detector coordinate for different angular modulation frequencies, different radii of the probing beam and
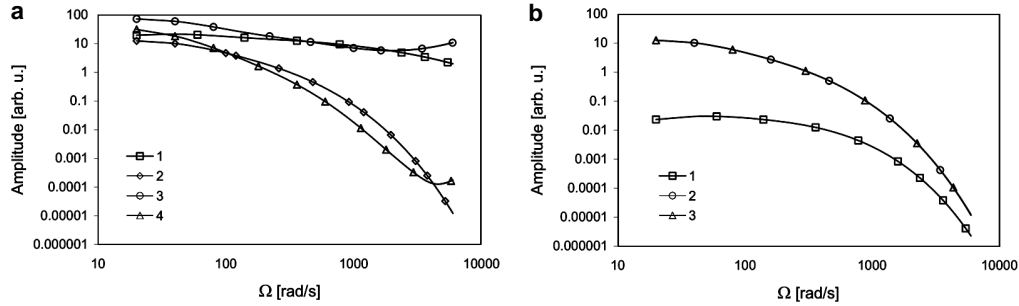

Fig. 4. Quadrant photodiode signal amplitude changes to modulation angular frequency: $a = 50\,\mu m$, $h = 200\,\mu m$ (curve 1); $a = 50\,\mu m$, $h = 1200\,\mu m$ (curve 2); $a = 500\,\mu m$, $h = 1200\,\mu m$ (curve 3); $a = 500\,\mu m$, $h = 2400\,\mu m$ (curve 4); others parameters are $z_D = 1.5$ m, $z_p = 0.505$ m, $z_l = 0.5$ m and $L = 0.5$ m – **a**. Components of the total normal signal: deflectional (curve 1) and phasial (curve 2) for $a = 50\,\mu m$, $h = 200\,\mu m$ (others parameters are $z_D = 1.5$ m, $z_p = 0.505$ m, $z_l = 0.5$ m and $L = 0.5$ m); curve 3 presents the total signal – **b**.
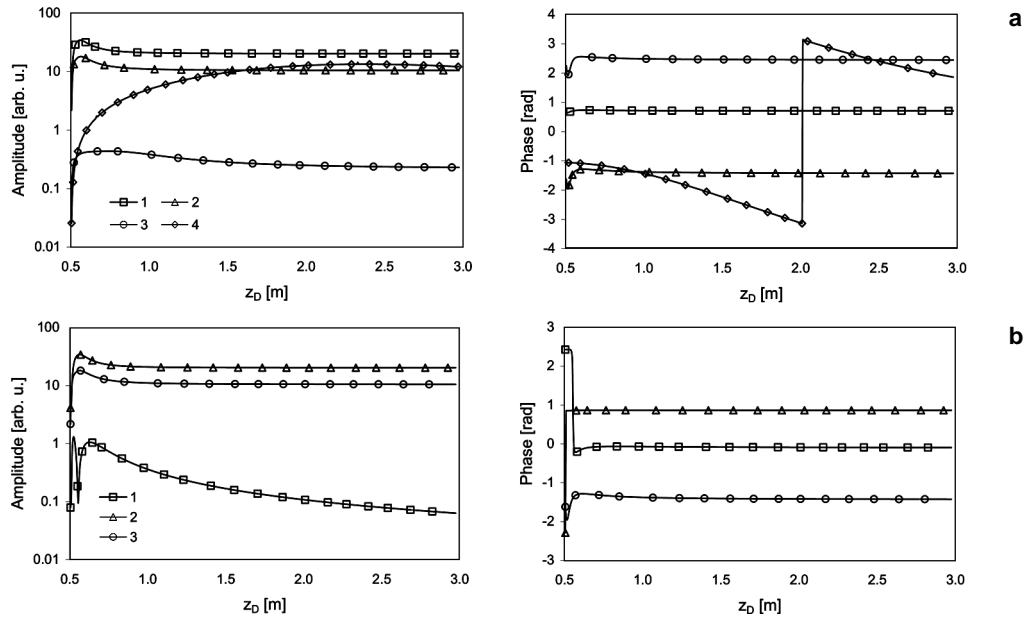

Fig. 5. Quadrant photodiode signal amplitude and additional phase shift changes relatively to detector position: $a = 50\,\mu m$, $\Omega = 60$ rad/s, $h = 200\,\mu m$ (curve 1); $a = 50\,\mu m$, $\Omega = 600$ rad/s, $h = 200\,\mu m$ (curve 2); $a = 50\,\mu m$, $\Omega = 600$ rad/s, $h = 1200\,\mu m$ (curve 3); $a = 500\,\mu m$, $\Omega = 600$ rad/s, $h = 1200\,\mu m$ (curve 1); pthers parameters are $z_p = 0.505$ m, $z_l = 0.5$ m and $L = 0.5$ m – **a**. Components of the total normal signal: deflectional (curve 1) and phasial (curve 2) for $a = 50\,\mu m$, $\Omega = 60$ rad/s, $h = 200\,\mu m$ ($z_p = 0.505$ m, $z_l = 0.5$ m and $L = 0.5$ m); curve 3 presents the total signal.
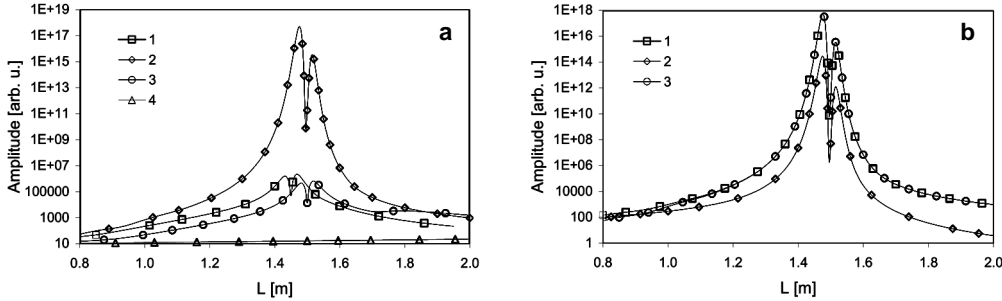
Fig. 6. Quadrant photodiode signal amplitude changes to beam waist position: $a = 50$ μm, $\Omega = 60$ rad/s, $h = 200$ μm (curve 1); $a = 50$ μm, $\Omega = 600$ rad/s, $h = 200$ μm (curve 2); $a = 50$ μm, $\Omega = 60$ rad/s, $h = 1200$ μm (curve 3); $a = 500$ μm, $\Omega = 600$ rad/s, $h = 1200$ μm (curve 4); others parameters are $z_D = 1.5$ m, $z_p = 0.505$ m, $z_l = 0.5$ m – **a**. Components of the total normal signal: deflectional (curve 1) and phasial (curve 2) for $a = 50$ μm, $\Omega = 600$ rad/s, $h = 200$ μm ($z_D = 1.5$ m, $z_p = 0.505$ m, $z_l = 0.5$ m); curve 3 presents the total signal.

its height over the sample. There is a rapid drop of the signal when the beam waist is over the detector and a rise when the beam waist is a bit in front of or behind it.

As can be seen from Fig. 6, for small values of the probing beam radii there is drop of the signal when the beam waist is over the detector, and rise when the beam waist is a bit in front of or a bit behind it. No such property of the signal is observed for large values of the probing beam radii. In this case, the curve increases monotonically.

Figure 7 shows the signal amplitude and additional phase shift dependence on the sample position of probing beam. The value of the signal decreases when we approach the detector. Phasial component gets smaller when the sample approaches the detector, but deflective component reaches a maximum when the beam waist is over the sample, and then decreases again.

On the graphs with phase change of photothermal signal from quadrant photodiode some discontinuities can be seen. They are the result of only "partial" phase normalization of the ambiguous component of the signal phase to the range $(0, 2\pi)$.

9. Conclusions

The influence of different experimental set-up parameters on signal value determined in photothermal investigation with mirage effect has been analysed in the work. The signal dependence on such parameters as probing beam radius, waist position, height over the sample surface and detector position was considered. The theory worked out, based on complex geometrical optics methods, offers the possibility of taking into account many other parameters (*e.g.*, probing beam modulation frequency), which are important for interpretations of measurement results. The so-called phasial and deflective components of normal signal created as a result of phase change and deflection of the beam, which is probed the one-dimensional field of the thermal wave propagated in the gas over the sample exited by harmonically modulated pumping
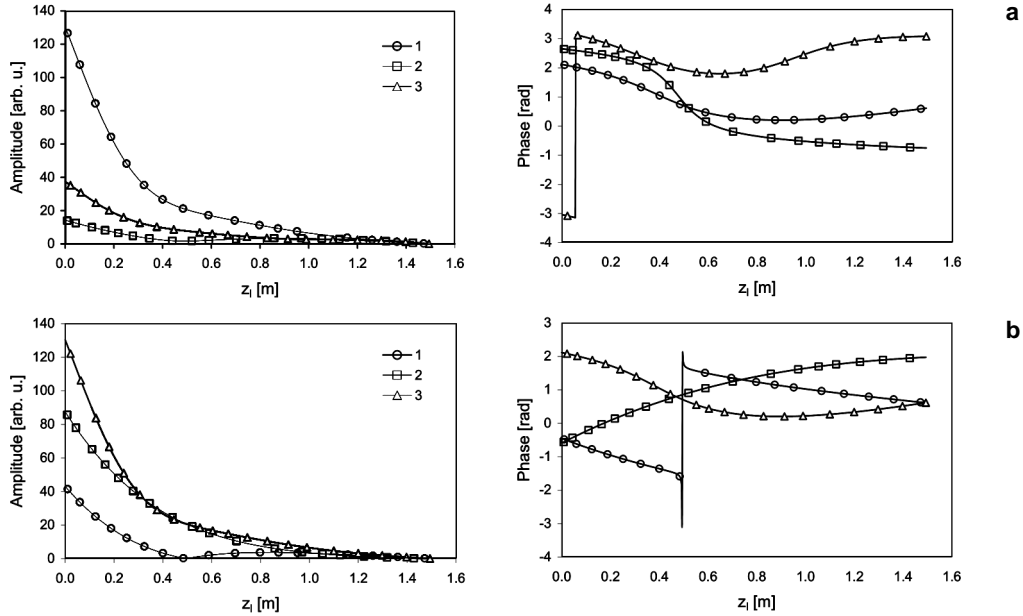
Fig. 7. Quadrant photodiode signal amplitude and additional phase shift changes relatively to sample position: $a = 50\ \mu m$, $\Omega = 60$ rad/s, $h = 200\ \mu m$ (curve 1); $a = 500\ \mu m$, $\Omega = 600$ rad/s, $h = 1200\ \mu m$ (curve 2); $a = 50\ \mu m$, $\Omega = 60$ rad/s, $h = 1200\ \mu m$ (curve 3); others parameters are $z_D = 1.5$ m and $L = 0.5$ m – **a**. Components of the total normal signal: deflectional (curve 1) and phasial (curve 2) for $a = 50\ \mu m$, $\Omega = 60$ rad/s, $h = 200\ \mu m$ ($z_D = 1.5$ m, $L = 0.5$ m); curve 3 presents the total signal.

beam, were considered. Quadrant photodiode detection has been analysed. Results are presented in analytical form and in the form of graphs and can be used for experimental set-up optimization. This means that by proper choice of the probing beam radius, waist position, height over the sample surface and detector position, probing beam modulation frequency we are able to increase the total normal signal or, if necessary, one component of it (phasial or deflective one) can be eliminated.

In the theory presented, we take into account for first time simultaneously two processes that are essential for photothermal signal creation – probing beam deflection and probing beam phase change. The dividision of the normal signal into deflective and phasial parts has rather theoretical meaning. Elimination of these parts from measurement signal will be very difficult or impossible. We present this dividision in order to make it possible for our readers to compare our theory with other ones, which take into account only one of the processes presented above. We use a new method for this type of calculation – complex geometrical optics method – and the results obtained are not fully equivalent to those of other calculations. From the graphs presented we can conclude that in many cases the results are qualitatively comparable with those of other theories.

The analytical formulas obtained are rather complicated, but, in our opinion, this is mainly due to the assumed method of detection, namely by a quadrant photodiode.

It needs additional integration of the probe beam intensity (expression (14)). Of course, it is possible to use other methods of detection. Some of them were analyzed in [8], but for phasial component of the normal signal only.

10. Appendix 1

The thermal wave really exists only over the sample surface, so relation (5) is to be rewritten as

$$\vartheta_g(x, t) = \Big[a_g + b_g \exp(-k_g x) \cos(\Omega t - k_g x + \varphi_g) \Big] \Big[H(z - z_l) - H(z_p - z) \Big].$$
(A1.1)

Because of the small value of the thermal wave amplitude b_g in standard experimental situation (of an order of mK) in relation (8) we neglect derivation over the z coordinate. This means that we neglect additional phase shifts caused by input and output of the probing beam into and out of the region with thermal wave. In such a situation, we obtain from relation (8):

$$x_1(\xi, \tau) = -\sqrt{2}\, b_g k_g n_0^2 s_T$$

$$\times \int_0^\tau \Bigg\{ (\tau - \tau') \exp\Big(-k_g x(\tau')\Big) \sin\Big(\Omega t - k_g x(\tau') + \varphi_g - \frac{\pi}{4} \Big)$$

$$\times \Big[H\Big(z(\tau') - z_l\Big) - H\Big(z_p - z(\tau')\Big) \Big] \Bigg\} d\tau'$$
(A1.2)

where from relations (3) and (4) in paraxial approximation we have

$$x(\tau') = \frac{z_{RC} + i n_0 \tau'}{z_{RC} + i z_D}, \quad z(\tau') = n_0 \tau'.$$
(A1.3)

Because of a linear character of relations (A1.3) the integral in (A1.2) is elementary one but it has very large and complicated shape. However, our calculations are not exact – we use paraxial approximation and perturbation calculus. So, if we have $(z_p - z_l) \ll z_D$ instead of exact value of the integral in (A1.2) we can apply its simplified value obtained by middle point method:

$$\int_{\tau_1}^{\tau_2} f(\tau, \tau') d\tau' \cong f(\tau, \tau_s)\, \tau_{pl}, \quad \tau_s = \frac{\tau_1 + \tau_2}{2}, \quad \tau_{pl} = \tau_2 - \tau_1.$$
(A1.4)

In our case, because of Heaviside's step functions in integral (A1.2), quantities τ_s and τ_{pl} depend on z_l and z_p (see formulas (8c)). It is clear that in this case the accuracy of the simplified integration can be easily controlled.

The same simplified method of integration is used in other places when integration over the τ' is needed. It is worth noting here that in some cases integrals are not elementary.

11. Appendix 2

The amplitude and the phase of probing beam on the detector surface (quadrant photodiode) can be written as:

$$A(z_D) \cong A_0(z_D)\Big[1 + a_1(z_D)\Big], \tag{A2.1}$$

$$\psi(z_D) \cong \psi_0(z_D) + \psi_1(z_D) \tag{A2.2}$$

where $A_0(z_D)$, $\psi_0(z_D)$ are expressed by Eq. (2) and $\psi_1(z_D)$ is described by Eq. (11); $a_1(z_D)$ from (A2.1) can be written as:

$$a_1(z_D) \;=\; -\frac{1}{2}\frac{\left(\dfrac{z_D - z_s}{n_0}\right)\dfrac{\partial P}{\partial \xi}\bigg|_{\xi = \xi_0}^{\tau_{pl}}}{1 + i\dfrac{z_D}{z_{RC}}} \tag{A2.3}$$

where $P(\xi)$ is expressed by (16b) and $z_s = n_0\tau_s$. Finally, the electric field distribution of probing beam on the surface of detector (quadrant photodiode) can be written as

$$u(\mathbf{r_D}) \cong A_0(z_D)\Big[1 + a_1(z_D)\Big]\exp\Big\{ik\Big[\psi_0(z_D) + \psi_1(z_D)\Big]\Big\}. \tag{A2.4}$$

We are allowed now to calculate the intensity distribution on that detector:

$$I(\mathbf{r_D}) \propto \big|u(\mathbf{r_D})\big|^2 \;=\; \Big|A_0(z_D)\Big[1 + a_1(z_D)\Big]\Big|^2\Big|\exp\Big\{ik\Big[\psi_0(z_D) + \psi_1(z_D)\Big]\Big\}\Big|^2. \tag{A2.5}$$

Correction to the phase and amplitude is complex, so it can be written as:

$$\psi_1(z_D) \;=\; \psi_{1R}(z_D) + i\psi_{1I}(z_D), \qquad a_1(z_D) \;=\; a_{1R}(z_D) + ia_{1I}(z_D), \tag{A2.6}$$

and we are given:

$$I(\mathbf{r_D}) \cong I_{0g}(\mathbf{r_D})\Big[1 - 2k\,\psi_{1I}(z_D) + 2a_{1R}(z_D)\Big] \;=\; I_{g0}(\mathbf{r_D}) + I_V(\mathbf{r_D}), \qquad \text{(A2.7)}$$

$$I_{0g}(\mathbf{r_D}) \;=\; A_0^2(z_D)\Big|\exp\Big[ik\,\psi_0(z_D)\Big]\Big|^2,$$

$$I_{Ag}(\mathbf{r_D}) \;=\; 2a_{1R}(z_D)\,I_{0g}(\mathbf{r_D}),$$

$$I_{\psi g}(\mathbf{r_D}) \;=\; -2k\,\psi_{1I}(z_D)\,I_{0g}(\mathbf{r_D}) \;=\; -2k\Big[\psi_{1dI}(z_D) + \psi_{1fI}(z_D)\Big]I_{0g}(\mathbf{r_D}) \quad \text{(A2.8)}$$

$I_{0g}(\mathbf{r_D})$ is the undisturbed Gaussian beam intensity distribution, but $I_V(\mathbf{r_D})$ represents changes in the probing beam intensity caused by its interaction with the thermal wave field. From relations (A2.8) we have

$$I_V(\mathbf{r_D}) \;=\; I_{gA}(\mathbf{r_D}) + I_{g\psi}(\mathbf{r_D}) \;=\; I_{gA}(\mathbf{r_D}) + I_{g\psi d}(\mathbf{r_D}) + I_{g\psi f}(\mathbf{r_D}). \qquad \text{(A2.9)}$$

This means that we can divide $I_V(\mathbf{r_D})$ into two parts: deflective and phasial ones. Deflective component of Gaussian beam intensity changes has the shape: $I_{gd}(\mathbf{r_D}) = I_{gA}(\mathbf{r_D}) + I_{g\psi d}(\mathbf{r_D})$ where $I_{gA}(\mathbf{r_D})$ – deflective component resulting from the Gaussian beam amplitude changes in the thermal wave field, $I_{g\psi d}(\mathbf{r_D})$ – a part of the deflective component arising from the Gaussian beam phase change connected with ray path moving. The last term in (A2.9) is a phasial component of the Gaussian beam intensity changes arising from the Gaussian beam phase change in the field of thermal wave.

In our case (lock-in measurements) only $I_V(\mathbf{r_D})$ is measured. Taking into account (A2.7) and (A2.8) we get:

$$S_n \;=\; 2K_d\mathrm{Re}\left[\left(\int_0^\infty - \int_{-h}^0\right)\mathrm{d}x_D\,a_1(z_D)I_{Vx}(\mathbf{r_D})\right] - 2K_d\mathrm{Im}\left[\left(\int_0^\infty - \int_{-h}^0\right)\mathrm{d}x_D\,k\,\psi_1(z_D)I_{Vx}(\mathbf{r_D})\right]$$
$$\text{(A2.10)}$$

where

$$I_{Vx}(\mathbf{r_D}) \;=\; \int_{-\infty}^\infty I_{0g}(\mathbf{r_D})\mathrm{d}y_D \;=\; I_m\exp\!\left(-f\,x_D^2\right),$$

$$I_m \;=\; \frac{z_R P_l}{\sqrt{\pi}\,a\,\sqrt{z_R^2 + (L - z_D)^2}}, \qquad\qquad \text{(A2.11)}$$

$$f \;=\; \frac{z_R^2}{a^2\Big[z_R^2 + (L - z_D)^2\Big]},$$

and P_l – the total power of undisturbed probing beam. Moreover, we need relations (A2.3) and (11), where we have:

$$P(\xi_0) = \sqrt{2}\, n_0^2 s_T b_g\, k_g \exp\left(-C_x x_D\right) \sin\left(\Omega t - C_x x_D + \varphi_g - \frac{\pi}{4}\right), \qquad \text{(A2.12)}$$

$$C_x = k_g\left(1 + i\frac{z_s}{z_{RC}}\right)\left(1 + i\frac{z_D}{z_{RC}}\right)^{-1}. \qquad \text{(A2.13)}$$

In all calculations, we assume that $z_D > z_p$, *i.e.*, quadrant photodiode is placed behind the sample.

11.1. Phasial component of the normal signal

Taking into account relation (A2.9) we have

$$S_{nf} = -2K_d \mathrm{Im}\left[\left(\int_0^\infty - \int_{-h}^0\right) \mathrm{d}x_D\, k\, \psi_{1f}(z_D) I_{Vx}(\mathbf{r_D})\right]. \qquad \text{(A2.14)}$$

where (comp. (11))

$$\psi_{1f}(z_D) = \frac{1}{2} n_0^2 s_T b_g\, \tau_{pl}\left[e^{\,i(\Omega t + \varphi_g - C_x x_D)} + e^{\,-i(\Omega t + \varphi_g - C_x x_D)}\right] e^{\,-C_x x_D}. \qquad \text{(A2.15)}$$

We neglect here constant component proportional to a_g – this component is not measured by lock-in technique. After calculating the proper integrals we are given:

$$S_{nf} = A_f \cos\left(\Omega t + \varphi_g - \varphi_f\right) \qquad \text{(A2.16)}$$

where

$$A_f = \frac{1}{2}\sqrt{\frac{\pi}{f}}\, K_d n_0 s_T b_g\, k\, I_m(z_p - z_l) \sqrt{(F_{1l} + F_{2l})^2 + (F_{2R} - F_{1R})^2}\,, \qquad \text{(A2.17)}$$

$$\tan\varphi_f = -\frac{F_{2R} - F_{1R}}{F_{1l} + F_{2l}}, \qquad \text{(A2.18)}$$

$$
\begin{aligned}
F_1 &= \exp\left\{\left[\frac{(1+i)C_x}{2\sqrt{f}}\right]^2\right\}\left\{1 - 2\mathrm{erf}\left[\frac{(1+i)C_x}{2\sqrt{f}}\right] + \mathrm{erf}\left[\frac{(1+i)C_x}{2\sqrt{f}} - h\sqrt{f}\right]\right\} \\
&= F_{1R} + iF_{1I}, \tag{A2.19}
\end{aligned}
$$

$$
\begin{aligned}
F_2 &= \exp\left\{\left[\frac{(1-i)C_x}{2\sqrt{f}}\right]^2\right\}\left\{1 - 2\mathrm{erf}\left[\frac{(1-i)C_x}{2\sqrt{f}}\right] + \mathrm{erf}\left[\frac{(1-i)C_x}{2\sqrt{f}} - h\sqrt{f}\right]\right\} \\
&= F_{2R} + iF_{2I}, \tag{A2.20}
\end{aligned}
$$

and $\mathrm{erf}(\xi)$ is the error function.

11.2. Deflective component of the normal signal

Deflective part of the normal signal in our case has two components, the first one comes from the diversion of the Gaussian beam in the thermal wave field (relations (13), (A2.1) and (A2.3)), and the second arises from the Gaussian beam phase change connected with ray path moving (relations (11), (A2.8) i (A2.9)).

For the first component calculation we have:

$$
S_{ndA} = 2K_d \mathrm{Re}\left[\left(\int_0^\infty - \int_{-h}^0\right)\mathrm{d}x_D a_1(z_D)I_{Vx}(\mathbf{r_D})\right]. \tag{A2.21}
$$

Taking into account relation (A2.3) we obtain:

$$
S_{ndA} = A_{dA}\cos(\Omega t + \varphi_g + \varphi_{dA}), \tag{A2.22}
$$

$$
A_{dA} = 2K_d\sqrt{(G_{1R} - G_{2R})^2 + (G_{1I} + G_{2I})^2}\,,
$$

$$
\tag{A2.23}
$$

$$
\tan\varphi_{dA} = -\frac{G_{1I} + G_{2I}}{G_{1R} - G_{2R}}
$$

where

$$G_1 = \frac{i}{2} \frac{(\tau_D - \tau_s)\tau_{pl}}{1 + i\dfrac{z_D}{z_{RC}}} n_0^2 s_T b_g k_g C_x I_m \exp\left[(i-1)^2 \frac{C_x^2}{4f}\right]$$

$$\times \left\{ \frac{2\sqrt{\pi}\,\mathrm{erf}\left[(i-1)\dfrac{C_x}{2\sqrt{f}}\right]}{2\sqrt{f}} - \frac{\sqrt{\pi}\,\mathrm{erf}\left[(i-1)\dfrac{C_x}{2\sqrt{f}} + h\sqrt{f}\right]}{2\sqrt{f}} + \frac{\sqrt{\pi}}{2\sqrt{f}} \right\}$$

$$= G_{1R} + iG_{1I}, \tag{A2.24}$$

$$G_2 = \frac{i}{2} \frac{(\tau_D - \tau_s)\tau_{pl}}{1 + i\dfrac{z_D}{z_{RC}}} n_0^2 s_T b_g k_g C_x I_m \exp\left[(i+1)^2 \frac{C_x^2}{4f}\right]$$

$$\times \left\{ \frac{2\sqrt{\pi}\,\mathrm{erf}\left[-(i+1)\dfrac{C_x}{2\sqrt{f}}\right]}{2\sqrt{f}} - \frac{\sqrt{\pi}\,\mathrm{erf}\left[-(i+1)\dfrac{C_x}{2\sqrt{f}} + h\sqrt{f}\right]}{2\sqrt{f}} + \frac{\sqrt{\pi}}{2\sqrt{f}} \right\}$$

$$= G_{2R} + iG_{2I}, \tag{A2.25}$$

For the second component calculation we have:

$$S_{ndf} = -2K_d \mathrm{Im}\left[\left(\int_0^\infty - \int_{-h}^0\right) dx_D\, k\, \psi_{1d}(z_D) I_{Vx}(\mathbf{r_D})\right] \tag{A2.26}$$

where

$$\psi_{1d}(z_D) = z_D n_0 \frac{x_D(\tau_D - \tau_s)}{z_{RC}^2} P(\xi_0)\tau_{pl}\left(1 + i\frac{z_D}{z_{RC}}\right)^{-2}. \tag{A2.27}$$

After calculating proper integrals we are given:

$$S_{ndf} = A_{df}\cos\left(\Omega t + \varphi_g + \varphi_{df} - \frac{\pi}{4}\right), \tag{A2.28}$$

$$A_{df} = 2K_d \sqrt{(H_{1I} - H_{2I})^2 + (H_{1R} + H_{2R})^2},$$

$$\tan \varphi_{df} = -\frac{H_{1R} + H_{2R}}{H_{1I} - H_{2I}}$$

(A2.29)

where

$$H_1 = \frac{\sqrt{2}}{2i} k\, z_D\, n_0^3 \frac{\tau_D - \tau_s}{z_{RC}^2} \frac{\tau_{pl}}{\left(1 + i\dfrac{z_D}{z_{RC}}\right)^2} I_m s_T b_g k_g$$

$$\times \left\{ \frac{\sqrt{\pi}(i-1)C_x}{4f^{3/2}} \exp\left[\frac{(i-1)^2 C_x^2}{4f}\right] \left[\mathrm{erf}\left(\frac{i-1}{2\sqrt{f}}C_x + h\sqrt{f}\right) - \mathrm{erf}\left(\frac{i-1}{2\sqrt{f}}C_x\right) \right] \right.$$

$$+ \frac{1}{2f} \exp\left[-(i-1)C_x h - fh^2\right]$$

$$\left. - \frac{\sqrt{\pi}(i+1)C_x}{4f^{3/2}} \exp\left[\frac{(i+1)^2 C_x^2}{4f}\right] \left[1 - \mathrm{erf}\left(\frac{i+1}{2\sqrt{f}}C_x\right)\right] \right\},$$

(A2.30)

$$H_2 = \frac{\sqrt{2}}{2i} k\, z_D\, n_0^3 \frac{\tau_D - \tau_s}{z_{RC}^2} \frac{\tau_{pl}}{\left(1 + i\dfrac{z_D}{z_{RC}}\right)^2} I_m s_T b_g k_g$$

$$\times \left\{ \frac{\sqrt{\pi}(i-1)C_x}{4f^{3/2}} \exp\left[\frac{(i-1)^2 C_x^2}{4f}\right] \left[1 - \mathrm{erf}\left(-\frac{i-1}{2\sqrt{f}}C_x\right)\right] \right.$$

$$+ \frac{1}{2f} \exp\left[(i+1)C_x h - fh^2\right] + \frac{\sqrt{\pi}(i+1)C_x}{4f^{3/2}} \exp\left[\frac{(i+1)^2 C_x^2}{4f}\right]$$

$$\left. \times \left[\mathrm{erf}\left(-\frac{i+1}{2\sqrt{f}}C_x\right) - \mathrm{erf}\left(-\frac{i+1}{2\sqrt{f}}C_x + h\sqrt{f}\right) \right] \right\}.$$

(A2.31)

References

[1] MURPHY J.C., AAMODT L.C., *Photothermal spectroscopy using optical beam probing: mirage effect*, Journal of Applied Physics **51**(9), 1980, pp. 4580–8.

[2] GLAZOV A., MURATIKOV K., *Photodeflection signal formation in thermal wave spectroscopy and microscopy of solids within the framework of wave optics. "Mirage" effect geometry*, Optics Communications **84**(5-6), 1991, pp. 283–9.

[3] AAMODT L.C., MURPHY J.C., *Photothermal measurements using a localised excitation source*, Journal of Applied Physics **52**(8), 1981, pp. 4903–14.

[4] BUKOWSKI R.J., BODZENTA J., MAZUR J., KLESZCZEWSKI Z., *Parameter Estimation in Photothermal Measurements with Photodeflective Detection*, [In] *Nondestructive Characterization of Materials VII, Part 1, Proceedings of the Seventh International Symposium on Nondestructive Characterization of Materials held in Prague, Czech Republic, June 1995*, Transtec Publications 1996, pp. 295–302.

[5] KRAWCOW JU.A., ORŁOW JU.I., *Geometrical Optics of the Nonhomogeneous Media*, WNT, Warszawa 1993 (in Polish).

[6] BUKOWSKI R.J., *Geometrical optics application in description of gaussian beam propagation in an optically homogenous medium*, [In] *Proceedings of the 2nd National Conference "Physical Basis of the Nondestructive Investigations"*, Gliwice Chapter of the Polish Physical Society and Institute of Physics of the Silesian University of Technology, Gliwice'97 (in Polish).

[7] BUKOWSKI R.J., *Mirage effect description in the frame of the complex rays optics* Proceedings of the SPIE **3581**, 1998, pp. 285–92.

[8] BUKOWSKI R.J., *Complex geometrical optics application in different methods of detection analysis in photothermal measurements*, Zesz. Nauk. Pol. Śl., Seria: Matematyka–Fizyka, z87, pp. 37–54 (1999) (in Polish).

[9] YARIV A., YEH P., *Optical Waves in Crystals: Propagation and Control of Laser Radiation*, Wiley, New York 1984.

[10] CARSLAW H.S.. JAEGER J.C., *Conduction of Heat in Solids*, Oxford University Press, Oxford 1959.

[11] Bodzenta J., Bukowski R., Kleszczewski Z., Mazur J., Pustelny B., *Thermal waves application in solids investigation*, Zesz. Nauk. Pol. Śl., Seria: Matematyka–Fizyka, z73, pp. 51–72 (1996) (in Polish).